

The Radial Temperature Distribution in Plasma cutting

1. Overview of Plasma Arc Cutting system [1]

Plasma cutting is a reliable, fast (the max. possible cut speed is 200 ipm), high-quality and low-cost method. Cut quality is better than oxyfuel. And the optimal cutting range is between 0.048 to 2 in for steel. It can be used on all conductive metals. But the repeatability is worse than laser and waterjet because of consumability of its torch components. The torch components should be replaced periodically because worn or damaged parts can cause gas and water leaks which can affect the cut quality.

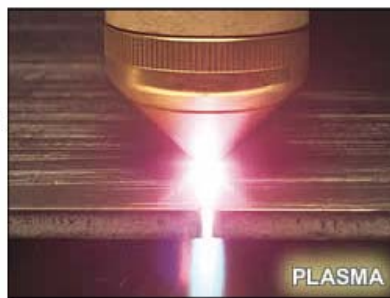


Figure 1. Plasma cutting

2. How does plasma arc cutting work and of its components with functions?

Plasma Arc Cutting uses a transferred arc to melt a conductive work-piece and a high speed gas jet removes the molten material [2]. Figure 2 shows main components of the plasma arc cutting system. This cutting system consists of a DC power supply capable of providing 200A, a remote high frequency starter, and the cutting torch. Instead of the work-piece, a water-cooled rotating copper ring serves as the anode. This allows the torch to be operated without actually cutting the work-piece and generating fumes. In other words, it allows operation of the torch without the cost or by-products associated with cutting material. Both the water cooling and a rotation speed of 200 rpm are needed to prevent damage to the anode.

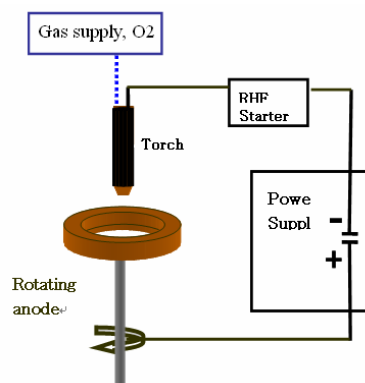


Figure 2. Components of Plasma Arc Cutting System

The internal torch components greatly influence cutting capability and cut quality and are therefore important. The components of the torch are the cathode, swirl ring, nozzle and shield cap in figure 3. The plasma gas flow through the nozzle and is given a swirl component by the swirl ring. A second gas flow, called shield gas flows between the nozzle and the shield cap. Electrons are supplied to the arc from the refractory metal insert through thermionic emission. When cutting with oxygen, hafnium is frequently used as the emitter because it can withstand the oxidizing atmosphere. The arc is constricted by the nozzle, swirling the plasma gas and further by shield gas flow. This constriction increases the arc current density, heat and velocity.

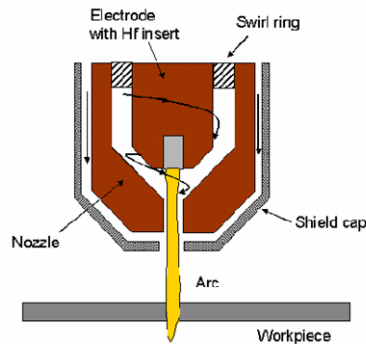


Figure 3. Internal component of cutting torch

3. Heat transfer to the anode

In order to achieve the high cutting speeds, very high heat fluxes must be present at the work-piece. These fluxes are typically on the order of $10^9 \text{ W} / \text{m}^2$ for many cutting systems. Figure 4 shows measured the radial temperature distribution at 4 mm from the torch tip. So I want to know the heat flux to the anode using this temperature distribution at 4mm from the torch. And usually 5mm is the distance between torch and work-piece. A boundary layer is less than half one mm and, the temperature at 4 mm can be thought one temperature using LTE assumption. But there exist non-LET condition near the anode surface. So I'd like to know the axial temperature change using appropriate assumption.

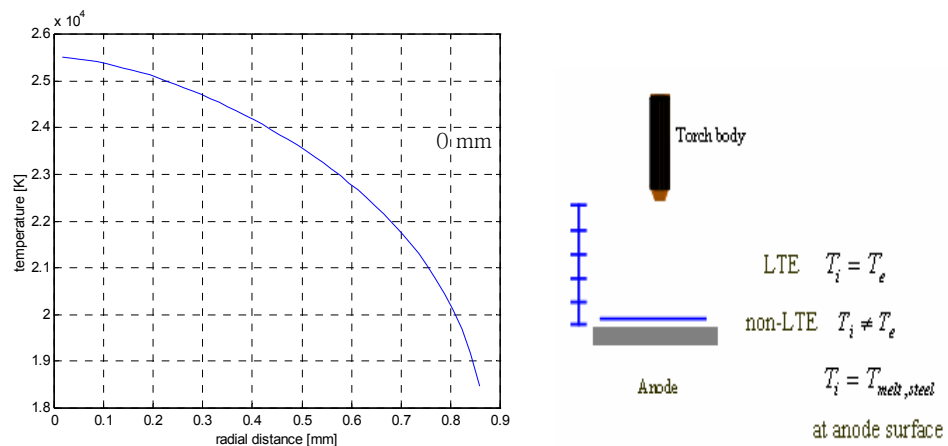


Figure 4. Radial temperature distribution at 4 mm from the torch tip

Figure 5 shows the axial temperature distributions of the electron (1) and heavy-species (2) over a distance from 4mm to 5mm from the torch for the free-burning arc with a 200A atmospheric pressure argon arc [3]. The anode is placed at the position 5 mm here. The electron temperature begins to separate from the heavy species temperature at a distance of 0.2 mm in front of the anode. The centerline anode electron temperature is close to 11,200 K. I assumed that axial temperature distribution of the oxygen arc at the previous slide follows this axial temperature drop using normalization. That is, when I take the temperature at 4 mm as one, the heavy particle temperature linearly decreases from 0.67 at 0.1mm to the anode temperature. And the electron temperature linearly drops to 0.87 at 0.2mm from the anode and to 0.79 at the surface.

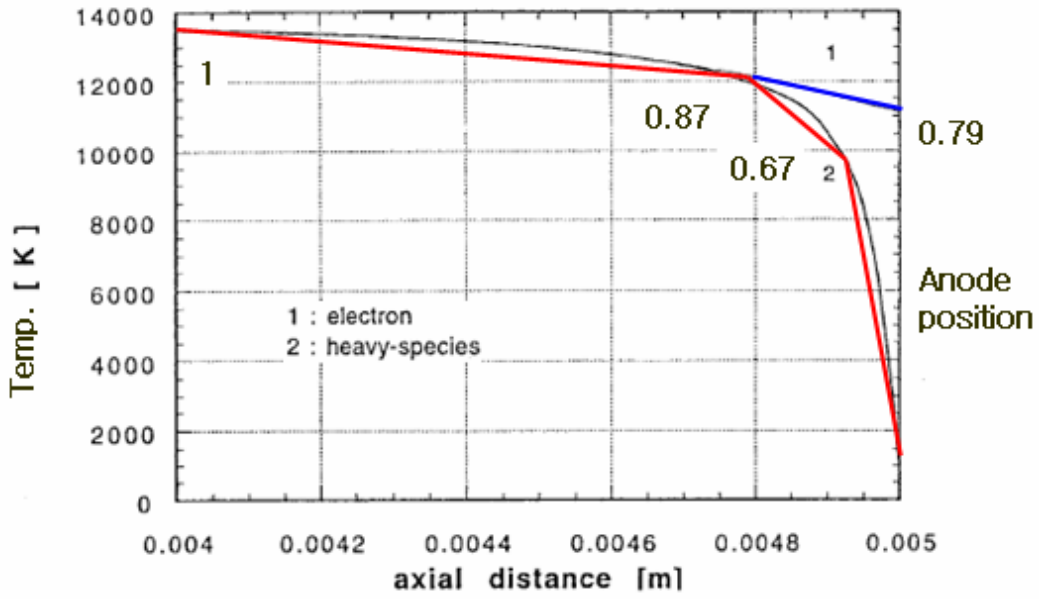


Figure 5. Axial temperature distribution of argon plasma between 4mm and 5mm

$$q_a = j\phi_w + \left(\frac{5}{2} \frac{k_B}{e} + \frac{\phi}{\sigma}\right) jT_e - K_h \frac{dT_h}{dx} - K_e \frac{dT_e}{dx} - j_i(\epsilon_i - \phi_w) \quad (2)$$

From the heat transfer to anode equation (2), here work function for copper is 4.67V. Most common metals can be roughly assumed to have a work function of around 4.5.

$$q_a = j\phi_w + \left(\frac{5}{2} + \frac{\phi}{\sigma} \frac{e}{k_B}\right) \frac{k_B}{e} jT_e - K_h \frac{dT_h}{dx} - K_e \frac{dT_e}{dx} - j_i(\epsilon_i - \phi_w) \quad (3)$$

After modifying the equation to (3), for electron temperatures around or exceeding 10,000 K in anode region, we can assume the term $\frac{\phi}{\sigma} \frac{e}{k_B}$ assumes a constant value of 0.703.

$$q_a = j\phi_w + 3.203 \frac{k_B}{e} jT_e - K_h \frac{dT_h}{dx} - K_e \frac{dT_e}{dx} - j_i(\epsilon_i - \phi_w) \quad (4)$$

The final heat flux equation is as in the equation (4).

$$j = \sigma E_x, \tag{5}$$

$$I = 2\pi \int_0^R j r dr = 2\pi E_x \int_0^R \sigma r dr \quad \text{and after discretizing it to} \quad E_x = \frac{I}{2\pi \sum_i \sigma_i r_i dr}$$

Where

and after discretizing it to

In order to get current density, I used relationship among current, electrical conductivity and electric field in equation 5. These two graphs in figure 6 show electrical and thermal conductivity [4].

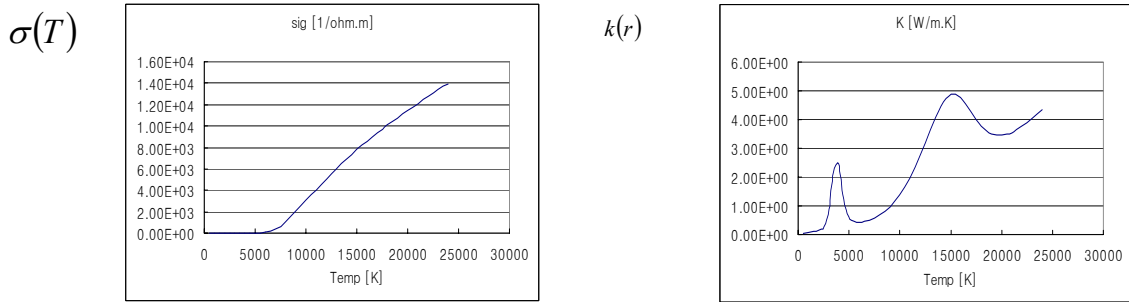


Figure 6. Oxygen properties (electrical conductivity and thermal conductivity)

The contribution of the ion recombination to the anode heat flux is negligibly small and has been accordingly ignored. The figure 7 shows Heat flux contributions to the anode in oxygen constricted arc. Dominant are the first three terms (electron condensation, electron enthalpy, and heavy particle conduction) in heat flux to the anode. Dotted magenta is total heat flux. The maximum of total heat flux to the anode is $1.6 \times 10^9 W / m^2$, which is similar to the expected heat flux to the anode. Green line is heavy particle conduction. Since, up to now, there is no published paper dealing with non-equilibrium condition experiment or numerical simulation, I cannot verify against other materials. So I want to compare it with that of the argon plasma gas as in figure 8.

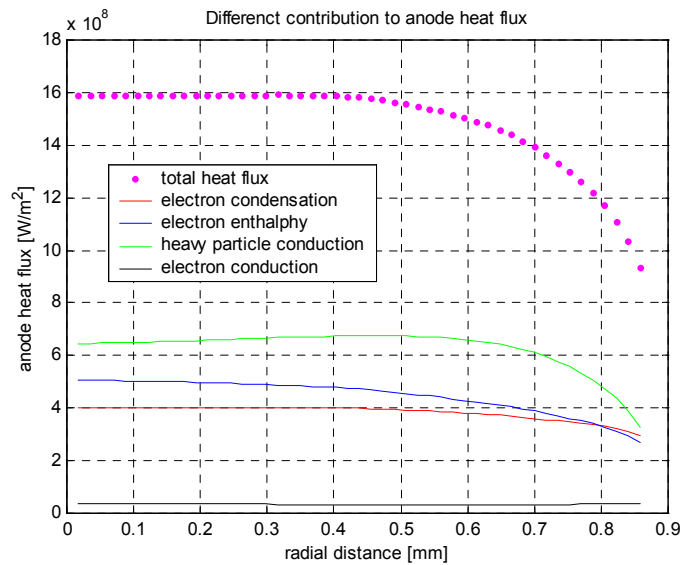


Figure 7. Heat flux contributions to the anode (Oxygen constricted arc)

This figure 8 shows the different contributions to the anode heat flux in case of argon gas for 200A [5]. Also the first three terms shows big contribution. But there are some differences comparing my result. At the previous slide, the heavy particle conduction is higher than others because the plasma gas is oxygen and has higher temperature than argon gas. So the temperature difference between near and at the anode is higher. Another difference lies in the shape of the heat flux. The reason is in chapter 5.

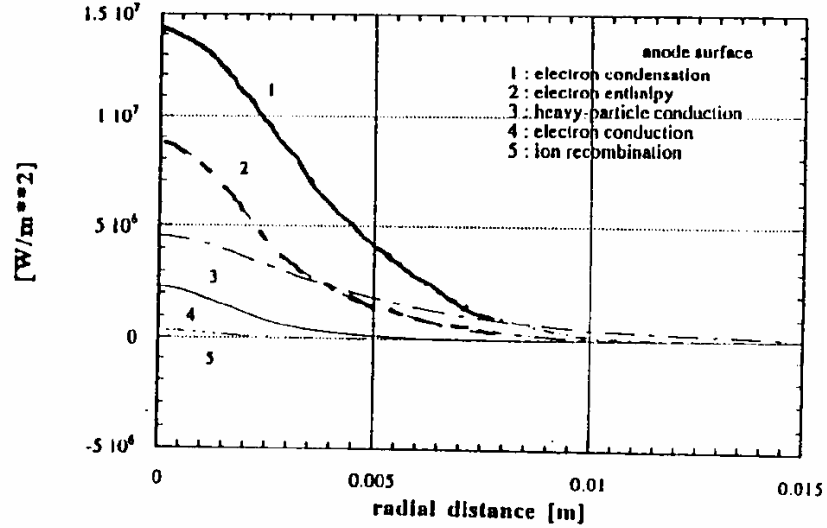


Figure 8. Heat flux contributions to the anode (Argon free-burning arc)

4. Elenbaas-Heller Equation for fully developed temperature profile

Using Elenbaas-Heller equation (6), fully developed radial temperature distribution in figure 9 was compared to its measured temperature.

$$\frac{1}{r} \frac{1}{dr} \left\{ r \kappa \frac{dT}{dr} \right\} = \lambda(T) - \sigma \cdot E^2 \quad (6)$$

After Disretization,

$$\frac{1}{r_i} \frac{1}{\Delta r} \frac{r_{i+1/2} \kappa_{i+1/2} \frac{T_{i+1} - T_i}{\Delta r} - r_{i-1/2} \kappa_{i-1/2} \frac{T_i - T_{i-1}}{\Delta r}}{\Delta r} = \lambda_i - \sigma_i E_i^2 \quad (7)$$

I used Gauss-Seidel method for numerical computation. As temperature change at each step, I updated κ (thermal conductivity) and σ (electrical conductivity), changing radius and got temperature distributing satisfying both (5) and (7)

The radiation properties are like bellows with respect to temperature.

$$\begin{aligned} \lambda(T) &= 0 & 0 \leq T \leq 4 \times 10^3 \text{ } ^\circ K \\ \lambda(T) &= 1.18512 \times 10^{10} [(T - 4000)/12800]^{4.795} \text{ ergs/cm}^3 \cdot \text{sec} & 4 \times 10^3 \text{ } ^\circ K \leq T \leq 16 \times 10^3 \text{ } ^\circ K \\ \lambda(T) &= 1.8641 \times 10^{16} \text{ ergs/cm}^3 \cdot \text{sec} & T > 16 \times 10^3 \text{ } ^\circ K \end{aligned}$$

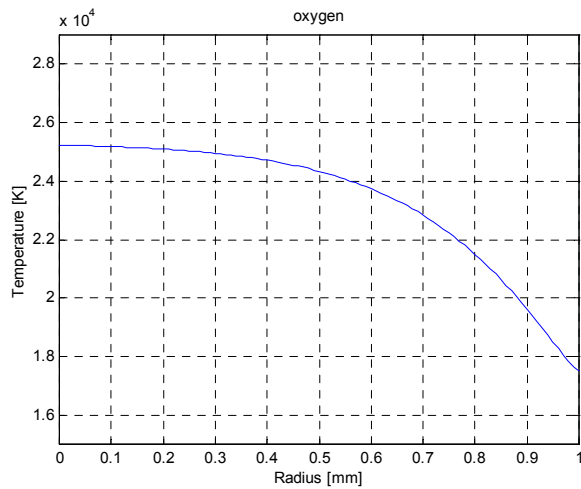


Figure 9. Fully developed temperature distribution using Elenbaas-Heller Equation.

Figure 10 shows radial temperature profiles at different axial distances from the nozzle. This figure clearly shows the under-expanded nature of the plasma jet leaving the torch nozzle. The arc quickly expands outward and the temperature decreases significantly in the first 1.5 mm after the nozzle exit. This is followed by a rapid increase in the temperature 2.5 mm from the nozzle tip and then a much slower axial temperature drop with which it is assumed that the temperature from 4 mm away form the nozzle tip is fully developed.

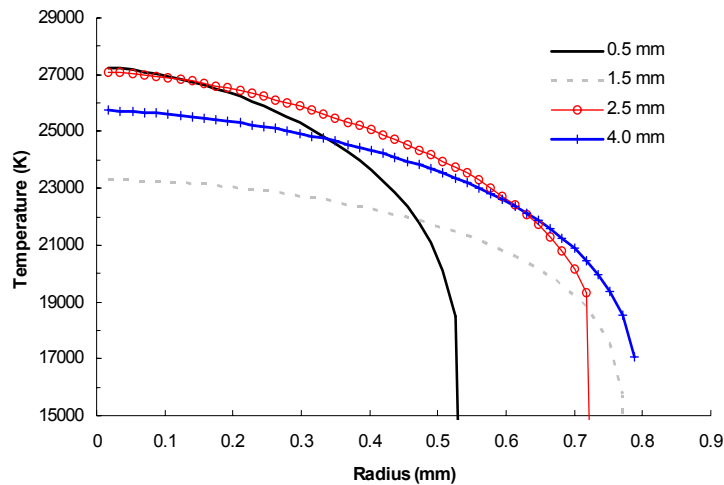


Figure 10. Radial temperature profiles at several axial locations from the nozzle exit plane.

The comparison between figure 9 and 10 (at 4 mm) shows good agreement in temperature distribution. Thus Elenbaas-Heller equation is a good assumption for producing representative temperature profiles of the positive arc column in a cylindrical tube.

References:

1. "Oxyfuel, plasma, laser, or waterjet?", NOMMA Education Foundation (NEF) NO. 6 August 2003
2. John Peters, "Effect of torch design and operating conditions on plasma properties in a plasma cutting system," PhD dissertation (2005)
3. Jiri Jenista, Joachim V. R. Heberlein, *Member, IEEE*, and Emil Pfender, "Numerical Model of the Anode Region of High-Current Electric Arcs," IEEE TRANSACTIONS ON PLASMA SCIENCE, VOL. 25, NO. 5, October (1997)
4. Boulos, Fauchais, and Pfender, Plenum Press, "Thermal Plasmas: Fundamentals and Applications," New York (1994)
5. JOACHIM HEBERLEIN, "Electrode Phenomena in Plasma Torches," Annals of the New York Academy of Sciences 891:14-27 (1999)